Journal of Magnetism and Magnetic Materials 378 (2015) 451–456

Contents lists available at ScienceDirect

Journal of Magnetism and Magnetic Materials

journal homepage: www.elsevier.com/locate/jmmm

Magnetic and thermodynamic properties of the lightly electron-doped manganite compound (Ca,Sr)$Mn_{0.95}Sb_{0.05}O_3$

Takahiro Fujiwara [a], Michiaki Matsukawa [a,*], Takahiro Aoyagi [a], Satoru Kobayashi [a], Haruka Taniguchi [a], Shigeki Nimori [b], Ramanathan Suryanarayanan [c]

[a] Department of Materials Science and Engineering, Iwate University, Morioka 020-8551, Japan
[b] National Institute for Materials Science, Tsukuba 305-0047,Japan
[c] Laboratoire de Physico-Chimie de L'état Solide, CNRS, UMR8182, Université Paris-Sud, 91405 Orsay, France

ARTICLE INFO

Article history:
Received 9 December 2013
Received in revised form
14 September 2014
Accepted 21 November 2014
Available online 26 November 2014

Keywords:
Magnetization reversal
Electron doped manganites
Chemical pressure effect

ABSTRACT

We report on the *dc* magnetization and *ac* magnetic susceptibility of the lightly electron-doped manganite compound $(Ca^{2+}_{1-x}Sr^{2+}_{x})Mn^{4+}_{0.9}Mn^{3+}_{0.05}Sb^{5+}_{0.05}O^{2-}_{3}$ ($x=0.0$, 0.05, 0.10, 0.15, 0.16, 0.17, and 0.2) with a fixed carrier content, to examine the effect of chemical pressure on magnetization reversal of this system. In a weak magnetic-field-cooled measurement, diamagnetic magnetization is observed for $x \leq 15\%$, which changes to positive values for $x > 15\%$. We present a magnetic phase diagram as a function of Sr concentration in several magnetic fields. The *ac* magnetic susceptibility measurement indicates the existence of magnetic frustration for the Sr substituted samples exhibiting diamagnetic behavior. To better understand the thermodynamic properties of this system, we have measured the specific heat as a function of temperature over a field cooling of 100 Oe. Our data show no anomalies associated with the temperature-dependent magnetization reversal, indicating the absence of long-range magnetic ordering.

1. Introduction

Extensive studies on magnetization reversal and negative magnetization in magnetic materials demonstrate the potential uses of these mechanisms in magnetic memory and related applications [1]. $CaMnO_3$, the end member of the $Ca_{1-x}La_xMnO_3$ system, undergoes a G-type antiferromagnetic transition around $T_N \sim 120$ K, accompanied by a weak ferromagnetic component [2], in which each Mn ion spin is antiparallel to those of its nearest Mn ion neighbors. In recent years, the electron-doped manganite system ($x < 0.5$) [3] has attracted much attention because of the possibility of observing a negative magnetoresistance effect in it similar to that observed in its counterparts, the so-called hole-doped manganites, with $x > 0.5$. The negative magnetization phenomena in manganites were originally reported in compounds with two sublattices of Mn ions and rare-earth ions (Nd, Gd, and Dy) [4–6]. Some of these studies were discussed on the basis of a ferrimagnetic scenario causing negative magnetization at temperatures below a particular compensation temperature, where Mn and some rare-earth sub-lattices are antiferromagnetically coupled. Previously, negative magnetization in $CaMnO_3$ with B-site substitution had been reported [7]. Recently, we demonstrated the influence of hydrostatic pressure on magnetic and transport properties in the lightly electron-doped manganite $CaMn_{1-x}Sb_xO_3$ [8]. Anomalous magnetization reversals were clearly observed for $x=0.05$ and 0.08 under field-cooled magnetization while the application of external pressure suppressed the negative magnetization. A theoretical work on lightly electron-doped manganite $CaMnO_3$ predicted that spin canting in the G-type antiferromagnetic structure is realized by electron doping through the double exchange mechanism [9,10]. The weak FM component observed in Ce-substituted $CaMnO_3$ is explained well by the spin-canting G-type AFM state with the double-exchange hopping of electrons. For the lightly electron-doped samples of $CaMn^{4+}_{1-2x}Mn^{3+}_{x}Sb^{5+}_{x}O_3$, we believe that a weak ferromagnetic trend in their *MT* curves is compatible with the present canted AFM scenario. The larger Sb^{5+} substitution at Mn^{4+} sites introduces local lattice distortion of $Mn^{3+}O_6$ associated with e_g-electron doping and then changes the orbital state of e_g-electron through the local Jahn–Teller (JT) effect. As a result, it gives rise to considerable variation in the local spin configuration at the nearest neighbor of its Sb ion, leading to the formation of diamagnetic clusters within its matrix. The canted AFM matrix stabilized by light electron doping contributes to a weak ferromagnetic component. Furthermore, the diamagnetic clusters are

* Corresponding author.
E-mail address: matsukawa@iwate-u.ac.jp (M. Matsukawa).

http://dx.doi.org/10.1016/j.jmmm.2014.11.068
0304-8853/

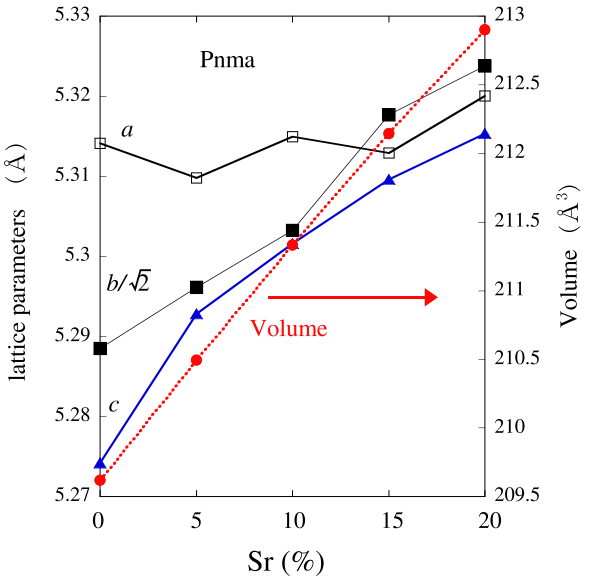

Fig. 1. Lattice parameters and unit-cell volume as a function of Sr estimated from X-ray diffraction patterns of $(Ca_{1-x}Sr_x)Mn_{0.95}Sb_{0.05}O_3$. The unit-cell volume is nearly proportional to the Sr content.

Table 1
EPMA analysis of $(Ca_{1-x}Sr_x)Mn_{0.95}Sb_{0.05}O_3$ (x=0.0, 0.15, 0.16, and 0.17).

Element nominal composition	Ca	Sr	Mn	Sb	O
$CaMn_{0.95}Sb_{0.05}O_3$	1.010	0.00	0.943	0.048	3.02
$(Ca_{0.85}Sr_{0.15})Mn_{0.95}Sb_{0.05}O_3$	0.845	0.164	0.927	0.048	3.03
$(Ca_{0.84}Sr_{0.16})Mn_{0.95}Sb_{0.05}O_3$	0.836	0.177	0.925	0.048	3.02
$(Ca_{0.83}Sr_{0.17})Mn_{0.95}Sb_{0.05}O_3$	0.830	0.187	0.918	0.047	3.04

simultaneously formed by local lattice deformation because of the substitution of Sb with its larger ionic radius.

In this paper, we report on the *dc* magnetization and *ac* magnetic susceptibility of the lightly electron-doped manganite compound $(Ca_{1-x}Sr_x)Mn_{0.95}Sb_{0.05}O_3$ with a fixed carrier content. Furthermore, to better understand the thermodynamic properties of this system, we conduct specific heat measurements for these compounds over a wide range of temperatures.

2. Experiment

Polycrystalline samples of $(Ca_{1-x}Sr_x)Mn_{0.95}Sb_{0.05}O_3$ (x=0.0, 0.05, 0.10, 0.15, 0.16, 0.17, and 0.2) were prepared using a solid-state reaction method. Here, Sr substitution at Ca sites causes a fixed carrier content according to the chemical formula $(Ca^{2+}_{1-x}Sr^{2+}_x)Mn^{4+}_{0.9}Mn^{3+}_{0.05}Sb^{5+}_{0.05}O^{2-}_3$. The stoichiometric mixtures of high purity $CaCO_3$, Mn_3O_4, Sb_2O_3 and $SrCO_3$ powders were calcined in air at 1000 °C for 24 h. The products were then ground and pressed into cylindrical pellets. The pellets were finally sintered at 1400–1450 °C for 12 h. X-ray diffraction data obtained using Rigaku Ultima IV revealed that all the samples had an almost single phase with an orthorhombic structure (*Pnma*) [11]. The lattice parameters and unit-cell volume estimated from X-ray diffraction patterns using the RIETAN-FP program are shown as a function of Sr content in Fig. 1. We note the linear relationship between the volume and Sr substitution at Ca sites in the present system, as previously reported in $(Gd_{0.08}Ca_{1-x}Sr_x)MnO_3$ [12]. X-ray photoemission spectroscopy on the $CaMn_{0.8}Sb_{0.2}O_3$ sample performed at room temperature strongly supports that the valence of

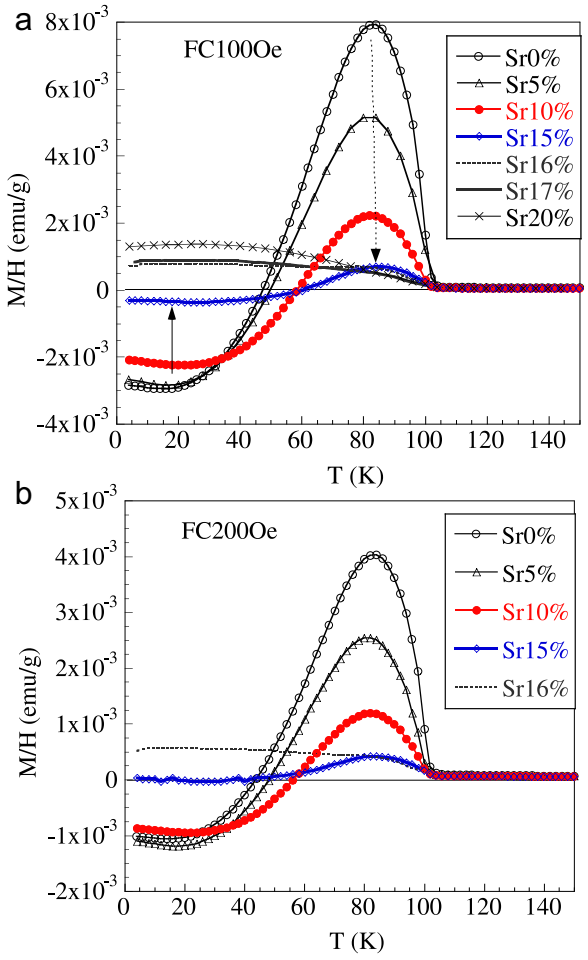

Fig. 2. Temperature dependence of the field-cooled magnetic susceptibility M/H for $(Ca_{1-x}Sr_x)Mn_{0.95}Sb_{0.05}O_3$ recorded at 100 Oe and 200 Oe, (a) and (b), respectively.

the Sb ion is 5+ [13]. The values obtained after electron probe micro analyzer (EPMA) analysis on the nominal samples with x=0.0, 0.15, 0.16, and 0.17 are listed in Table 1. We note that our samples prepared by the solid-state reaction method are close to the nominal composition and there is quite a small difference in the Mn content between the samples. The *dc* magnetization measurement was conducted using the commercial superconducting quantum interference device magnetometers at Iwate University and the National Institute for Materials Science (NIMS). The sample holder is attached with a nonmagnetic stainless steel rod provided by quantum design.

The dimensions of the sample used to measure the magnetic properties were typically 4.0 × 2.0 × 1.0 mm^3. The *ac* magnetic susceptibility measurement was obtained as a function of temperature for frequencies ranging from 1 Hz to 1000 Hz under an *ac* magnetic field of 5 Oe at NIMS. The specific heat measurement in the field-cooled mode was conducted at temperatures from 120 K down to 2 K using the physical property measurement system (quantum design PPMS).

3. Results and discussion

In Fig. 2(a), we demonstrate the effect of Sr substitution at Ca sites on the temperature-dependent magnetization for $(Ca_{1-x}Sr_x)Mn_{0.95}Sb_{0.05}O_3$($x$=0.0, 0.05, 0.1, 0.15, 0.16, 0.17, and 0.20). For the parent sample, on lowering the temperature, the magnetization shows a large enhancement near 80 K and diamagnetic

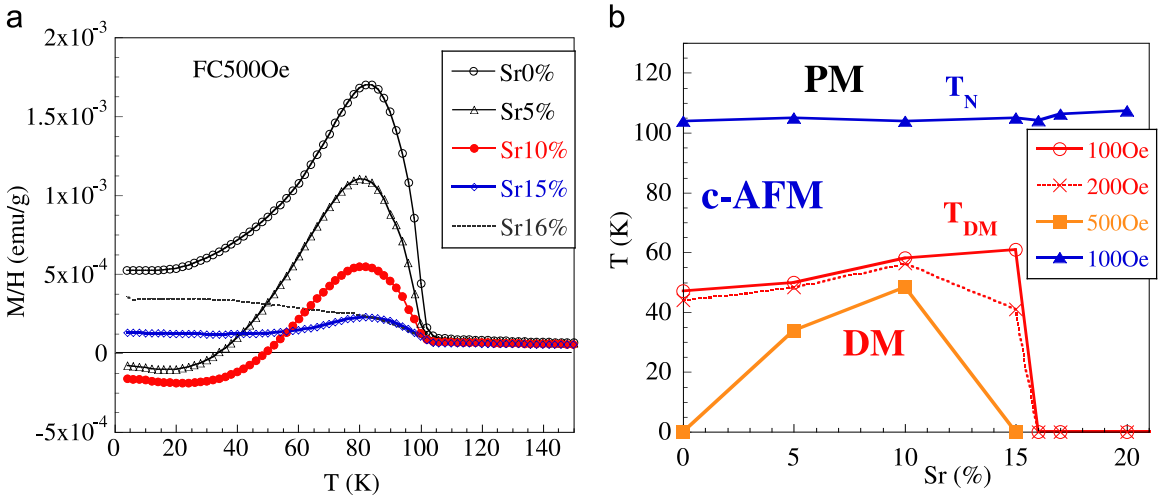

Fig. 3. (a) Temperature dependence of the field-cooled magnetic susceptibility M/H for $(Ca_{1-x}Sr_x)Mn_{0.95}Sb_{0.05}O_3$ recorded at 500 Oe. (b) Magnetic phase diagram of the Sr-substituted $(Ca_{1-x}Sr_x)Mn_{0.95}Sb_{0.05}O_3$ (x=0.0, 0.05, 0.1, 0.15, 0.16, 0.17, and 0.20), where PM, c-AFM, and DM denote paramagnetic, canted antiferromagnetic, and diamagnetic phases, respectively. T_{DM} and T_N represent the diamagnetic and canted antiferromagnetic transition temperatures, respectively.

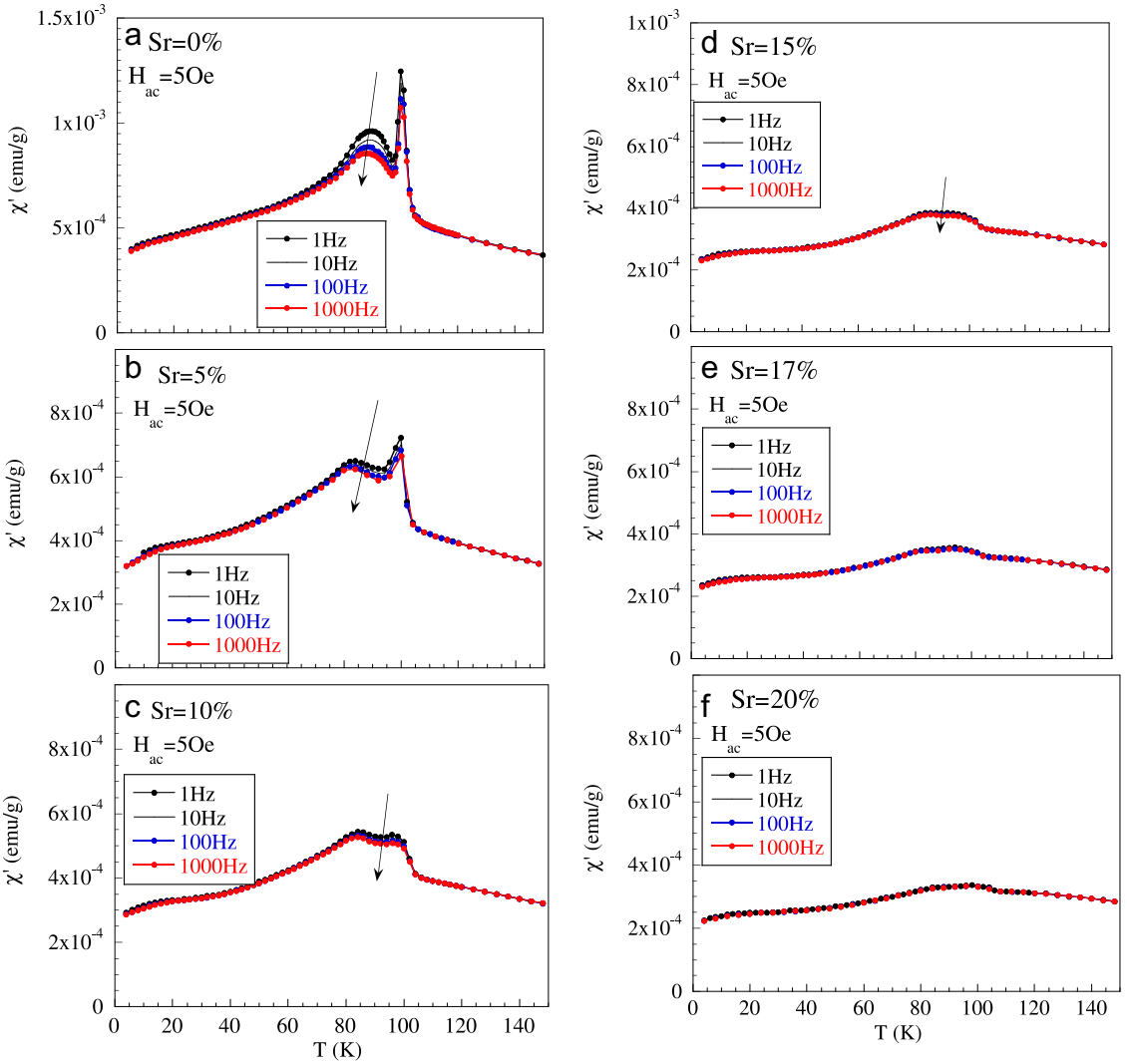

Fig. 4. Real part of the *ac* magnetic susceptibility for $(Ca_{1-x}Sr_x)Mn_{0.95}Sb_{0.05}O_3$ as a function of temperature collected at zero *dc* magnetic field for frequencies ranging from 1 Hz to 1000 Hz. (*a*) x=0.0, (*b*) x=0.05, (*c*) x=0.10, (*d*) x=0.15, (*e*) x=0.17, and (*f*) x=0.20. The amplitude of the *ac* magnetic field H_{ac} was set to 5 Oe. The arrows point in the direction of increasing frequency.

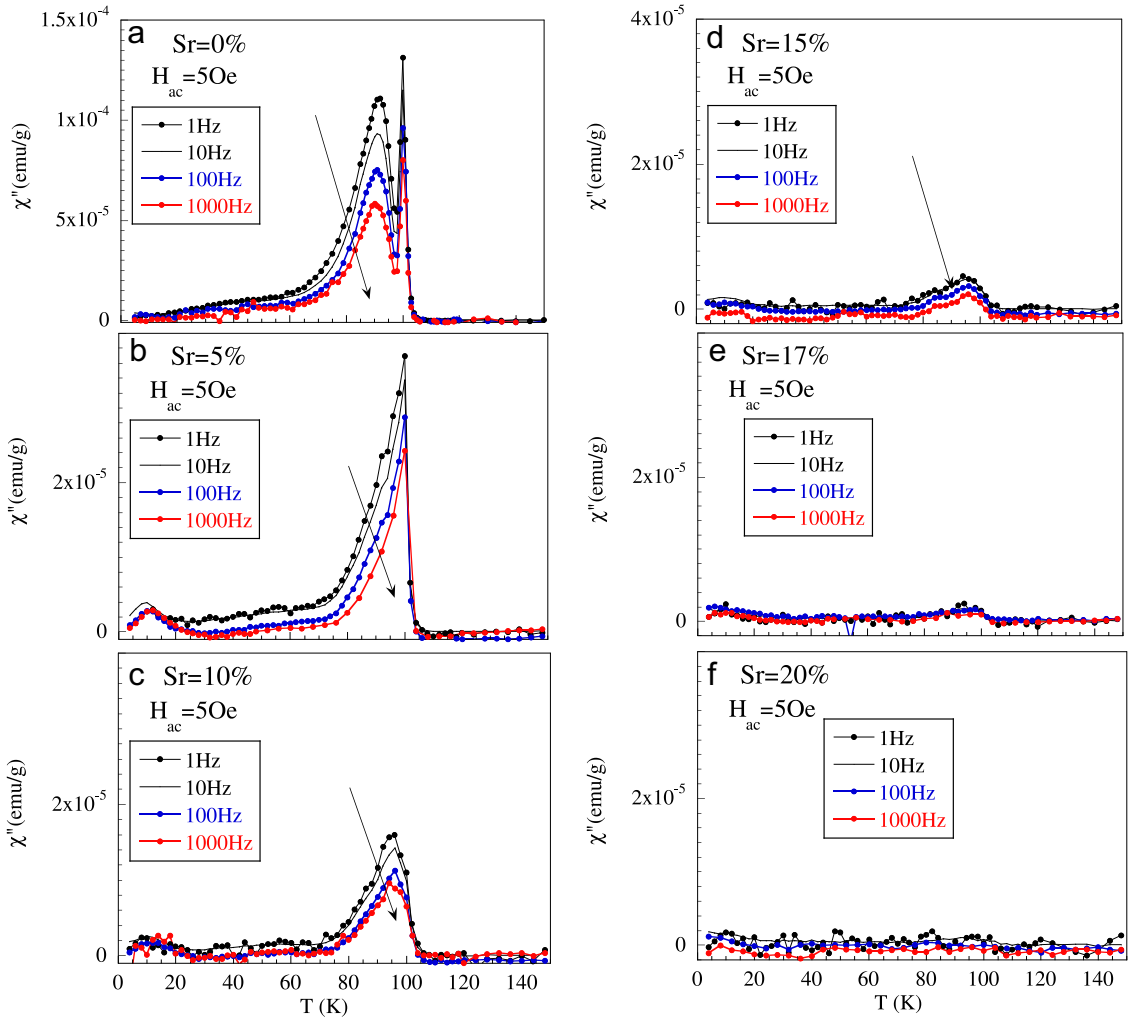

Fig. 5. Imaginary part of the *ac* magnetic susceptibility of $(Ca_{1-x}Sr_x)Mn_{0.95}Sb_{0.05}O_3$ as a function of temperature collected at zero *dc* magnetic field for frequencies ranging from 1 Hz to 1000 Hz. (*a*) $x=0.0$, (*b*) $x=0.05$, (*c*) $x=0.10$, (*d*) $x=0.15$, (*e*) $x=0.17$, and (*f*) $x=0.20$. The amplitude of the *ac* magnetic field H_{ac} was set to 5 Oe. The arrows point in the direction of increasing frequency.

behavior is observed at lower temperatures. The Sr substitution at Ca sites causes a strong suppression in the magnetic peak located around 80 K from 8×10^{-3} emu/g at $x=0.0$ through 5×10^{-3} emu/g at $x=0.05$ down to 2×10^{-3} emu/g at $x=0.10$. On the other hand, a negative value of the magnetization at 20 K is not significantly changed in the case of Sr content up to $x=0.10$. The effect of Sr substitution on the crystal structures of perovskite manganites $(Ca_{1-x}Sr_x)MnO_3$ and $(Gd_{0.08}Ca_{1-x}Sr_x)MnO_3$ causes a suppression of the Mn–O–Mn buckling [14,12]. It is revealed that in lightly electron doped manganites [12], the unit-cell volume increases linearly with increasing Sr substitution at Ca sites, which is caused not by the expansion of the Mn–O bond length but by the suppression of the tilting of the MnO_6 octahedra. Furthermore, our lattice data exhibit a linear relationship between volume and Sr content as shown in Fig. 1(a). In the case of low Sr content, the Sr ions are distributed within the canted AFM matrix, contributing to a weak ferromagnetic component. If the Sr substitution at Ca sites gives rise to a suppression of the buckling of Mn–O–Mn bonds, it results in the suppression of the magnetic peak. A further increase in Sr ion contents above 10% affects diamagnetic clusters occupying small regions around the Sb sites, and finally, the addition of Sr beyond 15% suppresses the diamagnetic magnetization. As mentioned previously in the Introduction, for the lightly electron doped sample of $CaMn^{4+}_{0.95}Mn^{3+}_{0.05}Sb^{5+}_{0.05}O_3$, the larger Sb^{5+} substitution at Mn^{4+} sites introduces e_g-electron and causes local lattice distortion of $Mn^{3+}O_6$ at the nearest neighbor of its Sb ion. The resultant local lattice deformation changes the orbital state of e_g-electron through the local JT effect. As a result, it gives rise to considerable variation in the local spin configuration at the nearest neighbor of its Sb ion, leading to the formation of diamagnetic clusters within its matrix. The diamagnetic clusters are formed by local lattice deformation because of the substitution of Sb with its larger ionic radius.

We suspect that the tilting of the $Mn^{3+}O_6$ octahedron near the Sb ion is relaxed by the higher Sr substitution, resulting in a decrease in the negative component. One interesting feature is that the disappearance of negative magnetization accompanies a collapse of the clear peak in the magnetization curve. In a similar way to the case of 100 Oe, the magnetization curves measured at 200 Oe for Sr=0%, 5% and 10% show magnetization reversal and their lower temperature values reach similar negative values although their peaks are quite different between the samples. For comparison, in Fig. 3(a), we present the magnetization data for $(Ca_{1-x}Sr_x)Mn_{0.95}Sb_{0.05}O_3$ measured at 500 Oe. For a relatively higher field, a diamagnetic state is suppressed but the phenomenon of magnetization reversal survives for Sr=5% and 10%. At a relatively high field of 500 Oe, the low-temperature magnetization curve of the Sr10% sample retains a more negative value than the

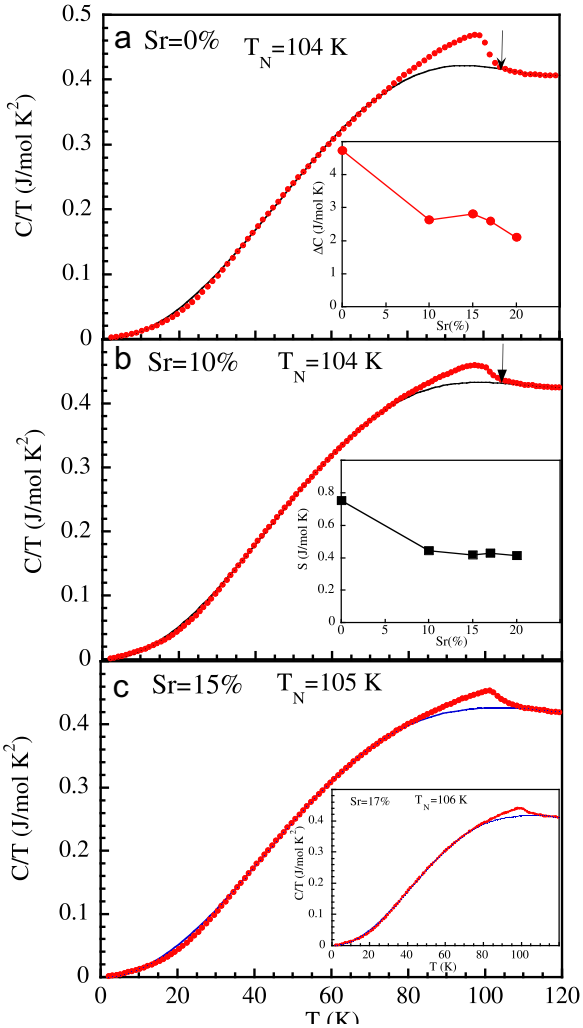

Fig. 6. C/T vs. T for $(Ca_{1-x}Sr_x)Mn_{0.95}Sb_{0.05}O_3$ measured under a field cooling of 100 Oe. (a) $x=0$, (b) $x=0.1$ and (c) $x=0.15$ (inset of (c) $x=0.17$). The solid curves denote the lattice contribution estimated from a polynomial approximation. The insets of (a) and (b) represent the magnetic heat jump ΔC and the magnetic entropy S_{mag} associated with the magnetic transition, respectively.

data of the lower Sr samples. This finding indicates that the Sr ion acts as the pinning center of diamagnetic clusters, preventing the rearrangement of their spins in the direction of applied field. The higher Sr substitution at Ca sites suppresses Mn–O–Mn buckling, deleting magnetization reversal, while the lower Sr substitution maintains a diamagnetic state at low temperatures. Furthermore, magnetization reversal of all the samples studied is completely suppressed when the applied field exceeds a field of 1000 Oe (not shown here). In terms of the total magnetic energy, we expect that the system is stable to align its magnetic moment along the applied magnetic field when the applied field reaches a moderately higher value. The magnetic phase diagram of $(Ca_{1-x}Sr_x)Mn_{0.95}Sb_{0.05}O_3$ established is summarized in Fig. 3(b).

Next, we conducted *ac* magnetic susceptibility measurements for $(Ca_{1-x}Sr_x)Mn_{0.95}Sb_{0.05}O_3$ ($x=0.0$, 0.05, 0.1, 0.15, 0.17, and 0.20), to clarify the dynamical effect on the diamagnetic state. The temperature dependence of the real and imaginary parts, χ' and χ'', is registered at zero *dc* magnetic field with increasing frequency f ranging from 1 Hz to 1000 Hz, as shown in Figs. 4 and 5. For the parent Sr0% sample, a sharp peak in the *ac* magnetic susceptibility is observed around 100 K, which is in good agreement with the *dc* magnetic measurement [8]. Upon increasing f, a second peak of χ' and χ'' located at 90 K shifts slightly towards lower temperatures. For lower values of Sr doping up to 10%, the amplitude of χ'' shows a strong decay with increasing frequency. When the Sr content exceeds 15%, the frequency dependence of the *ac* magnetic susceptibility almost disappears. The frequency dependence of the *ac* magnetization shows the signature of a spin-glass-like character; however, a substantial decrease in the peak in χ'' with increasing f is in contrast to the behavior of a conventional spin-glass system [16], as previously indicated in the phase-separated $Pr_{0.7}Ca_{0.3}MnO_3$ [17]. The *ac* magnetic susceptibility measurement of the lower Sr substituted samples suggests the existence of magnetic frustration between diamagnetic clusters and the canted antiferromagnetic matrix. On the other hand, for the Sr17% and Sr20% samples, the lack of frequency dependence of the *ac* magnetization is related to their weak ferromagnetic behavior under *dc* magnetization.

To further understand the thermodynamic properties of this system, we performed specific heat measurements over a wide range of temperatures under a field cooling of 100 Oe. Fig. 6 shows the specific heat as a function of temperature from 2 K to 120 K for $(Ca_{1-x}Sr_x)Mn_{0.95}Sb_{0.05}O_3$ ($x=0$, 0.1, 0.15, and 0.17). Here, the lattice contribution C_l is estimated roughly from a polynomial approximation as previously reported in manganites [15]. ΔC represents the maximum value of the magnetic contribution $C-C_l$ and the magnetic entropy is estimated by integrating $(C-C_l)/T$ with respect to T. We observe clear anomalies associated with a magnetic transition near T_N but no visible changes in the specific heat data at temperatures where the diamagnetic behaviors appear. Our thermodynamic data strongly support that the temperature-dependent magnetization reversal accompanies no long-range magnetic ordering. It is expected from these findings that short-range magnetic clusters around Sb ions have a close relationship with the appearance of the observed weak diamagnetism. For the Sr-substituted samples, both the magnetic heat jump and the magnetic entropy do not change significantly. In particular, we do not find distinct differences in thermodynamic properties between the diamagnetic Sr15% sample and the weakly ferromagnetic Sr17% sample.

4. Summary

We have demonstrated the magnetic and thermodynamic properties of the lightly electron-doped manganite compound $(Ca_{1-x}Sr_x)Mn_{0.95}Sb_{0.05}O_3$ ($x=0.0$, 0.05, 0.1, 0.15, 0.16, 0.17, and 0.20) with a fixed carrier content, to examine the effect of chemical pressure on magnetization reversal of this system. In the investigated system, there exits a linear relationship between the volume and the fraction of Sr substitution at Ca sites. In a weak magnetic-field-cooled measurement, the temperature-dependent negative magnetization appears for $x \leq 15\%$, changing to positive values for $x > 15\%$. We checked using EPMA analysis that our samples are close to the nominal composition and there is quite a small difference in the Mn content between the samples. We established a magnetic phase diagram as a function of Sr concentration under a field cooling of 100 Oe, 200 Oe and, 500 Oe. The lower Sr substitution maintains a diamagnetic state at low temperatures but the higher Sr substitution at Ca sites suppresses Mn–O–Mn buckling, deleting magnetization reversal.

Next, we conducted *ac* magnetic susceptibility measurements for this system, to clarify the dynamical effect on the diamagnetic state. The *ac* magnetic data indicate the existence of magnetic frustration accompanied by the progressive formation of diamagnetic clusters within the AFM matrix under decreasing temperature. For the Sr17% and Sr20% samples, the lack of frequency dependence of the *ac* magnetization is related to their weakly ferromagnetic properties under *dc* magnetization. To further understand the thermodynamic properties of this system, we

performed specific heat measurements over a wide range of temperatures under a field cooling of 100 Oe. However, the specific heat data do not reveal any magnetic phase transition associated with the temperature-dependent magnetization reversal.

References

[1] Y. Ren, T.T.M. Palstra, D.I. Khomskii, E. Pellegrin, A.A. Nugroho, A.A. Menovsky, G.A. Sawatzky, Nature 396 (1998) 441.
[2] J.B. MacChesney, H.J. Williams, J.F. Potter, R.C. Sherwood, Phys. Rev. 164 (1967) 779.
[3] H. Chiba, M. Kikuchi, K. Kasuba, Y. Muraoka, Y. Syono, Solid State Commun. 99 (1996) 499.
[4] F. Bartolome, J. Herrero-Albillos, L.M. Garcia, J. Bartolome, N. Jaouen, A. Rogalev, J. Appl. Phys. 97 (2005) 10A503.
[5] O. Pena, M. Bahout, K. Ghanimi, P. Duran, D. Gutierrez, C. Moure, J. Mater. Chem. 12 (2002) 2480.
[6] C.A. Nordman, V.S. Achutharaman, V.A. Vasko, P.A. Kraus, A.R. Ruosi, A. M. Kadin, A.M. Goldman, Phys. Rev. B 54 (1996) 9023.
[7] R. Ang, Y.P. Sun, Y.Q. Ma, B.C. Zhao, X.B. Zhu, W.H. Song, J. Appl. Phys. 100 (2006) 063902.
[8] Y. Murano, M. Matsukawa, S. Ohuchi, S. Kobayashi, S. Nimori, R. Suryanarayanan, K. Koyama, N. Kobayashi, Phys. Rev. B 83 (2011) 054437.
[9] C. Zener, Phys. Rev. 82 (1951) 403; P.G. deGennes, Phys. Rev. 118 (1960) 141.
[10] H. Ohnishi, T. Kosugi, T. Miyake, S. Ishibashi, K. Terakura, Phys. Rev. B 85 (2001) 165128.
[11] V. Poltavets, K. Vidyasagar, M. Jansen, J. Solid State Chem. 177 (2004) 1285.
[12] S. Hirano, J. Sugiyama, T. Noritake, T. Tani, Phys. Rev. B 70 (2004) 094419.
[13] T. Fujiwara, M. Matsukawa, S. Ohuch, S. Kobayashi, R. Suryanarayanan, S. Nimori, J. Kor. Phys. Soc. 62 (2013) 1925.
[14] O. Chmaissem, B. Dabrowski, S. Kolesnik, J. Mais, D.E. Brown, R. Kruk, P. Prior, B. Pyles, J.D. Jorgensen, Phys. Rev. B 64 (2001) 134412.
[15] J.E. Gordon, R.A. Fisher, Y.X. Jia, N.E. Phillips, S.F. Peklis, D.A. Wright, A. Zettl, J. Magn. Magn. Mater. 171–181 (1998) 856.
[16] C.A.M. Mulder, A.J. van Duyneveldt, J.A. Mydosh, Phys. Rev. B 23 (1981) 1384.
[17] I.G. Deac, J.F. Mitchell, P. Schiffer, Phys. Rev. B 63 (2001) 172408.